

3 **Metasomatized lithospheric mantle for Mesozoic giant gold deposits**
4 **in the North China Craton**

5 Zaicong Wang*, Huai Cheng, Keqing Zong, Xianlei Geng, Yongsheng Liu, Jinhui Yang,
6 Fuyuan Wu, Harry Becker, Stephen Foley, and Christina Yan Wang

7 *Email: zaicongwang@cug.edu.cn

8

9 **This file includes:**

- 10 **1. Analytical methods**
- 11 **2. Data quality of gold abundances and sample heterogeneity**
- 12 **3. Supplementary notes**
 - 13 **1) Gold contents in mantle xenoliths of the NCC**
 - 14 **2) Discrepancy between previous and new values on peridotites**
 - 15 **3) Gold contents in mantle-derived basalts**
 - 16 **4) High contents of water and volatiles in the 130-120 Ma basalts**
- 17 **4. Figures DR1-10**
- 18 **5. References**

19

20 **Note that the data sources are in another Data Repository Excel file.**

21 **Table DR1:** Major and trace elements, gold and PGEs contents and published Os-Sr-Nd-Hf isotopes in
22 mantle xenoliths from the NCC.

23 **Table DR2:** Major and trace elements, gold and PGEs contents and published Os-Sr-Nd-Hf-Pb
24 isotopes in the basalts.

25 **Table DR3:** Compiled literature data on mantle peridotite xenoliths from North China Craton.

26

27 **1. Analytical methods**

28 Visibly altered surfaces of basalts were removed with a rock saw. Cut surfaces were
29 abraded with silica emery paper and washed with 18.2Ω Milli-Q (Nanopure) water, and
30 subsequently dried overnight. Rock pieces of about 100 grams were crushed into small chips
31 and processed to fine powder using an agate disc mill. This procedure avoids possible metal
32 contamination from sample processing.

33 We modified previous analytical methods for gold and PGE contents (Fischer-Gödde et
34 al., 2011) and have established in Wuhan for different types of geological rocks (Cheng et al.,
35 2019). The bulk rock gold and PGE contents of xenoliths and basalts were determined after
36 Carius tube digestion in reverse aqua regia and chromatography separation: PGE by isotope
37 dilution methods and gold by two independent methods of standard addition and internal
38 standardization of gold to platinum (Cheng et al., 2019). After addition of a suitable amount
39 of mixed ^{191}Ir - ^{99}Ru - ^{194}Pt - ^{105}Pd and ^{185}Re spike solutions, about 2 grams of powder of each
40 sample was digested by reverse aqua regia (5 ml of 14 M HNO₃ and 2.5 ml of 9 M HCl) in
41 pre-cleaned Carius tubes at 240 °C for 3-4 days. The digested sample solutions were
42 transferred to centrifuge tubes, and 6 M HCl was used to rinse the Carius tube twice, and then
43 combined with the sample solution. After centrifugation, the supernatant solution was
44 completely transferred to weighed Teflon beakers and 6 M HCl was further used to rinse the
45 centrifuge tubes and transferred to the Teflon beakers. These processes ensure complete
46 recovery of Au and PGEs, which is important for quantitative determination of gold if the
47 standard addition method is applied (Cheng et al., 2019).

48 About one quarter of each sample solution was weighed and converted to chloride for
49 chemical separation. Chemical separation followed techniques described previously (Cheng et
50 al., 2019; Fischer-Gödde et al., 2011), and gold, Ir, Ru, Pt, Pd and Re were separated from the
51 matrix by cation exchange chromatography using 10 ml of pre-cleaned Eichrom 50W-X8
52 (100-200 mesh) resins. The samples were dissolved in 10 ml of a mixture of 0.5 M HCl - 40%
53 (V/V) acetone and loaded on the cation resin. 20 ml 0.5 M HCl - 40% (V/V) acetone was

54 collected for complete recovery (> 99%) of Au and PGEs. Afterwards, the eluent was dried
55 down to 0.5-1 ml.

56 The chemical purification procedure removed most matrix, except for some Cr, which
57 can be abundant (hundreds of ppm or more) in mantle xenoliths and basalts. To avoid the
58 potential effect of remaining matrix, two independent methods were used to determine the Au
59 contents: 1) internal standardization of gold to platinum, which is precisely determined by
60 isotope dilution and 2) standard addition which eliminates the effect of remaining matrix. For
61 the standard addition method, the sample solution was quantitatively separated into three
62 fractions and 1.25 M HCl and/or the gold standard solution with known concentration was
63 added (Cheng et al., 2019).

64 The samples in 1.25 M HCl solutions were measured by high sensitivity sector-field
65 inductively coupled plasma mass spectrometry (Thermo Scientific® Element II) at the State
66 Key Laboratory of Geological Processes and Mineral Resources, China University of
67 Geosciences, Wuhan. The detection limit of instrument was about 0.8 ppt for Au. The
68 monitored intensity of ^{181}Ta was low and the potential oxide interference of ^{181}TaO on ^{197}Au
69 (monitored $^{181}\text{Ta}/^{197}\text{Au} < 0.001$) was negligible in the routine measurement conditions with
70 Ta/TaO ratio of 0.002. The total procedural blanks were very low for gold ($\approx 5\pm 5$ pg, 2sd,
71 n=20), which resulted in low detection limits of our analytical methods. The abundances of Ir,
72 Pt and Re by isotope dilution were obtained with Au from the same aliquots. The sample
73 solution was further purified by anion resin for Ru and Pd (Cheng et al., 2019).

74 **2. Data quality of gold abundances and sample heterogeneity**

75 Accurate analysis of geological samples with low gold concentrations is very
76 challenging. Application of aqua regia and Carius tubes achieved low total procedural blanks
77 (Cheng et al., 2019; Fischer-Gödde et al., 2011). In our methods, the total procedural blanks
78 were only 5 ± 5 (2sd) pg for gold and resulted in low detection limits (Figure DR1). The data
79 quality of gold abundances was extensively evaluated in this study.

80 Gold concentrations were obtained by two independent methods: internal
81 standardization and standard addition. The values from the two methods are consistent within

82 a few percent (Table DR1-2; Figure DR2a). Geological reference materials with variable
83 compositions and their replicates such as TDB-1, BHVO-2 and GPt-2 have been analyzed and
84 the results showed the high precision and accuracy of the analytical methods (5-15%, 2sd)
85 (Cheng et al., 2019). For example, the replicates of TDB-1 by our method displayed a mean
86 value of 6.1 ± 0.7 ppb (2sd, n=20), similar to the certified 6.3 ± 1.0 ppb (2sd) and those analyzed
87 by nickel sulfide-fire assay (6.2 ± 0.6 ppb, 2sd, n=20) (Richardson and Burnham, 2002) and
88 HF-acid digestion (6.3 ± 1.7 ppb, 2sd, n=21) (Pitcairn et al., 2015). UB-N was determined
89 using internal standardization methods, and the gold content ranged from 1.0-1.7 ppb with a
90 mean value of 1.49 ± 0.52 ppb (2sd, n=11) (Fischer-Gödde et al., 2011). Our results were 1.1-
91 1.4 ppb with a mean of 1.2 ± 0.16 ppb (2sd, n=4). The gold in BHVO-2 is 1.1-1.4 ppb with a
92 mean of 1.3 ± 0.3 ppb (2sd, n=7). Overall, the typical analytical uncertainty for gold contents is
93 about 5-10 % (2sd) but can be larger (20-50%) for samples with very low gold contents of <
94 0.1 ppb (Table DR1-2; Figure DR2b).

95 Sample heterogeneity is often thought as a critical issue for Au and PGE contents in
96 ultramafic and mafic rocks. Thus, we have measured replicates of many peridotites and
97 basalts. For five basalts and three mantle xenoliths, the aqua regia solutions from the same
98 digestion were repeatedly purified via column separation and measured, and the results show
99 identical results, indicating excellent reproducibility of the gold data (Table DR1-2; Figure
100 DR3a). Replicates of eleven basalts and three mantle xenoliths were measured and they show
101 consistent results within uncertainty, indicating the negligible effect of sample heterogeneity
102 (Figure DR3b). PGE data have been available for most mantle xenoliths (Chu et al., 2009; Liu
103 et al., 2011) and our new PGE data are mostly similar to previous values, except for a few
104 samples with very low PGE contents, indicating the comparability of the PGE and Au data
105 between previous work and this study (Table DR1-3).

106 **3. Supplementary notes**

107 **3.1. Gold contents in mantle xenoliths of the NCC**

108 Mantle peridotites and pyroxenites, as well as experimental data (Brenan et al., 2016;
109 Mungall and Brenan, 2014), have constrained the magmatic behavior of PGEs, Au, Re, Cu

110 and S during partial melting, melt transport and refertilization, with sulfide melt-silicate melt
111 partition coefficients decreasing in the order: PGE > Au > Cu > S ≈ Re (e.g., Fischer-Gödde
112 et al., 2011; Lorand et al., 2008; Wang and Becker, 2015a, b; Wang et al., 2013). High-degree
113 melting would lead to high contents of Os-Ir-Ru (compatible) in refractory peridotites but low
114 Pd, Au, Cu and S contents with an increasing depletion in the order of Pd < Au < Cu < S
115 (variably incompatible), e.g., low Pd/Ir and Au/Pd (e.g., Becker et al., 2006; Fischer-Gödde et
116 al., 2011; Lorand et al., 2013; Luguet et al., 2007). Subsequent melt refertilization with
117 sulfide precipitation often enriches the refractory peridotites in incompatible Pd, Cu, Au and S,
118 leading to the elevation of Pd/Ir and Au/Pd (Fischer-Gödde et al., 2011; Lorand et al., 2008;
119 Lorand et al., 2013; Maier et al., 2012). A higher extent of enrichment of Au relative to PGE
120 is expected if strong melt/fluid metasomatism is involved, as reflected by peridotite xenoliths
121 from the Kaapvaal craton (e.g., Finsch and Venetia samples with high S contents of 280-1240
122 ppm and high Au/Pd_N of > 1 to 13, Maier et al., 2012).

123 The SCLM under the NCC metasomatized mainly by subduction materials is often
124 assumed to be the main gold source for the 130-120 Ma giant gold deposits (e.g., Goldfarb
125 and Groves, 2015; Li et al., 2012; Tan et al., 2018; Zhu et al., 2015). Gold contents in the
126 SCLM are of fundamental importance for understanding the formation of Mesozoic gold
127 deposits and could be directly represented by mantle xenoliths hosted in kimberlites and
128 basalts. The gold and PGE contents of many peridotite xenoliths hosted in Paleozoic
129 kimberlites (Mengyin and Fuxian) (Li et al., 2011; Zhang et al., 2008), Mesozoic basalts
130 (Xinyang) (Zheng et al., 2005) and Cenozoic basalts, e.g., Hebi, Shanwang (Zheng et al.,
131 2005), Wangqing (Orberger et al., 1998) and Hannuoba (Chu et al., 1999; Fischer-Gödde et
132 al., 2011) have been reported before. These data show a large range from 0.5-38.3 ppb Au
133 with a median value of 3.5 ppb (Figure DR4 and DR5), which is clearly higher than the
134 median 1.2 ppb of mantle peridotites worldwide (n=508, typical range of < 0.6 to 2 ppb)
135 (Saunders et al., 2018).

136 Mantle xenoliths from Hebi (Liu et al., 2011; Sun et al., 2012; Zheng et al., 2005;
137 Zheng et al., 2007), Mengyin and Fuxian (Zhang et al., 2008) are mostly highly refractory
138 harzburgites with low Al₂O₃ contents and high Mg# and show Neoarchean to

139 Paleoproterozoic Os model ages. These features reflect that they are the relics of ancient
140 lithospheric mantle after high-degree melt extraction. However, these harzburgites display
141 strong enrichment of light REE (Zheng et al., 2005), radiogenic Sr-Nd isotopes and high S
142 contents, suggesting that they have experienced subsequent extensive metasomatism with
143 sulfide precipitation. Previous data by NiS fire assay-ICPMS show high gold contents and
144 high Au/Pd_(N) in these refractory xenoliths (Zhang et al., 2008; Zheng et al., 2005). Mineral
145 separates of olivine and chromite from Mengyin xenoliths display surprisingly high gold
146 contents up to 6.2-16.9 ppb and high Au/Pd_(N) of 16-21 (Zhang et al., 2008). The Mesozoic
147 basalt-hosted Xinyang peridotite xenoliths (Zheng et al., 2005) and Cenozoic basalt-hosted
148 Shangwang (Zheng et al., 2005) and Wangqing xenoliths (Orberger et al., 1998) similarly
149 show high and variable gold contents (Figure DR5). These results could be interpreted as
150 evidence for an inherently gold-rich SCLM beneath the NCC from Archean to present
151 (Griffin et al., 2013), distinct from other mantle domains worldwide, including those with
152 strong mantle metasomatism, like Kaapvaal mantle xenoliths and other locations (Fischer-
153 G  dde et al., 2011; Maier et al., 2012; Saunders et al., 2018).

154 However, the Cenozoic Hannuoba basalt-hosted peridotites, which contain many
155 sulfides (Gao et al., 2002) show low gold contents of mostly 1-2 ppb (Chu et al., 1999;
156 Fischer-G  dde et al., 2011). Considering the highly variable gold contents in previous data
157 and their great importance, the well-characterized mantle xenoliths from Hebi, Mengyin and
158 Shanwang with published S, Cu and PGE contents (Chu et al., 2009; Liu et al., 2011) were
159 analyzed for gold in this study. The selected Mengyin peridotite and pyroxenite xenoliths
160 show strong enrichment of light REE and high S contents (Chu et al., 2009; Li et al., 2011),
161 which are the result of metasomatism between the Archean and 480 Ma. However, our new
162 data show only 0.06-0.50 ppb Au, as well as low Pd, Cu and Re contents (Chu et al., 2009),
163 suggesting limited recharge of Pd, Au and Cu by sulfur-bearing metasomatism. These gold
164 contents are significantly lower than the previously reported 3-6 ppb in peridotite xenoliths
165 from the same location. Similarly, Hebi harzburgites with ancient Os model ages and elevated
166 La/Yb_(N) also display low gold contents of 0.03-0.11 ppb (Figure 2). Note that in this study,
167 the low gold contents in Mengyin and Hebi harzburgite xenoliths are coupled with low Pd, Cu

168 and Re contents in the same samples (Figure 2). The elevated Au/Pd in some samples
169 suggests that metasomatism did replenish some chalcophile elements by sulfide precipitation,
170 but the low Au contents indicate that the amount was limited.

171 As for peridotite xenoliths from other Cenozoic basalts in the eastern NCC, Shanwang
172 xenoliths show Os isotopic compositions similar to abyssal peridotites (representing present-
173 day convecting mantle) (Chu et al., 2009). Combined with Sr-Nd-Hf isotopes, they suggest
174 that the lithosphere sampled by Shanwang peridotite xenoliths was derived from convecting
175 upper mantle during the Mesozoic or Cenozoic, after the destruction of the NCC (Chu et al.,
176 2009). These samples do not show enrichment of Pd and Re relative to compatible PGE such
177 as Os, Ir and Ru (Chu et al., 2009). Our new results for gold contents are 0.02-1.78 ppb with a
178 median value of 0.7 ppb (n=19), lower than previous values (3.4 to 6.7 ppb). Importantly, the
179 new gold analyses are also consistent with Pt, Pd and Cu contents. The contents and patterns
180 of PGE, Au, Cu and S are indistinguishable with fertile mantle (Figure 2, DR4).

181 Therefore, our high-precision new data from Hebi, Mengying, Shanwang mantle
182 xenoliths, as well as the previous gold data from Hannuoba mantle xenoliths (reflecting the
183 metasomatized ancient SCLM and juvenile SCLM under the NCC) indicate no substantial
184 enrichment of Au relative to Pd and Cu contents in the same samples. They suggest that the
185 NCC is not inherently rich in gold and that mantle metasomatism between the Archean and
186 480 Ma and replacement by juvenile lithospheric mantle did not lead to strong enrichment of
187 gold in the SCLM.

188 **3.2. Discrepancy between previous and new values on peridotites**

189 The PGEs contents in this study are generally consistent with previous values but gold
190 displays obvious discrepancy. The gold and PGE contents in peridotite xenoliths from Hebi,
191 Mengyin and Shangwang have been measured before and also by this study (Figure DR5).
192 This gives us an opportunity to better compare the obtained data. As discussed above, sample
193 heterogeneity is not the issue because the replicates show repeatable gold and PGEs contents
194 (Figure DR3). Instead, the different data quality for gold contents may be the main reason.
195 Previous gold data from North China Craton were highly variable and mostly higher than

196 other regions worldwide (mostly 3-16 ppb, Figure DR5). However, the peridotite xenoliths
197 from Hannuoba show low gold contents of 1-2 ppb, which are more reasonable for fertile
198 mantle rocks (Fischer-Gödde et al., 2011). The high values were mainly obtained by NiS fire
199 assay pre-concentration method, but the latter was by aquia-regia solution with rather low
200 blanks (a few pg). It is well known that the NiS fire assay method often shows variable levels
201 of procedural blanks for Au (e.g., from <0.1 ng to several ng), sometimes similar or even
202 higher than samples (e.g., Barefoot and Van Loon, 1999; Gros et al., 2002; Oguri et al., 1999).
203 It implies that it is difficult to accurately measure samples with low gold contents sometimes.
204 Given the inconsistent values in previous studies, we thus have set up the robust analytical
205 methods and used a lot of international geological reference materials to test our data quality
206 (Cheng et al., 2019). Our new methods led to very low gold blanks of a few pg, which makes
207 it possible to measure samples with rather low gold contents. The gold contents in this study
208 were also obtained by two independent methods for one sample, and they are consistent with
209 a few percent (Figure DR2).

210 **3.3. Gold contents in mantle-derived basalts**

211 The basalts in this study include high Mg# (71-75), hydrous, isotopically enriched 130-
212 120 Ma basalts, and isotopically depleted < 110 Ma basalts (Figure DR6). The former are
213 Yixian, Sihetun, Fangcheng and Feixian basalts (Gao et al., 2008; Huang et al., 2017; Liu et
214 al., 2008). They are from the northern (Yixian, Sihetun) and southern (Feixian, Fangcheng)
215 margins of the eastern NCC, where pre-existing Paleozoic and Triassic subduction occurred
216 and probably affected the SCLM.

217 The 130-120 Ma basalts from SCLM of the North China Craton have been intensively
218 studied in the past (Gao et al., 2008; Geng et al., 2019a; Geng et al., 2019b; Huang et al.,
219 2017; Liu et al., 2008; Meng et al., 2015; Xia et al., 2013; Zhang et al., 2002). They are
220 characterized by high water contents (Geng et al., 2019b; Xia et al., 2013), arc-like trace
221 element patterns (Figure DR7) and radiogenic Sr-Nd-Hf-Os isotopes (Gao et al., 2008; Huang
222 et al., 2017; Liu et al., 2008; Meng et al., 2015). These features have been interpreted to be
223 the accumulated consequences of multiple stages of metasomatism of the SCLM (e.g., Meng

et al., 2015; Wu et al., 2019; Zhang et al., 2002). Although crustal contamination could lead to similar isotopic features, but it is not a viable explanation for 130-120 Ma basalts from the North China craton. The main lines of evidence are: 1) Mesozoic mantle-derived rocks (130-120 Ma), irrespective of basalts (Meng et al., 2015; Zhang et al., 2002), lamproites (Ma et al., 2016) and gabbros (Xu et al., 2004) all show similar Sr-Nd isotopes (Wu et al., 2019); 2) such Sr-Nd isotopes hardly change for different rocks with variable SiO₂ (e.g., Ma et al., 2014; Wan et al., 2019); 3) Ratios of trace elements such as Nb/U and Ce/Pb are similar to MORBs rather than mixture with crustal materials and also do not support the model of crustal contamination (e.g., Ma et al., 2016); 4) 130-120 Ma basalts contain high abundances of water and other volatiles (Geng et al., 2019a; Geng et al., 2019b; Xia et al., 2013) which cannot result from the high-grade metamorphic crust. All these results support that the 130-120 Ma were originated from metasomatized and hydrated mantle.

The primitive magmas were derived from melting of metasomatized and hydrated SCLM and erupted around 120-125 Ma, coeval with or slightly before the peak formation of giant gold deposits (130-120 Ma). The high PGE contents (this study) and radiogenic Os isotopes (Gao et al., 2008; Huang et al., 2017) suggest that these primitive basalts dominantly resulted from the metasomatized and fusible components of the metasomatized SCLM. Discrete gold grains may be present in veins of metasomatized peridotites (Tassara et al 2017), and such fusible rocks could be entered into the melts. Therefore, the 130-120 Ma basalts are of great importance in constraining the degree of gold enrichment in the metasomatized and hydrated SCLM, and as an analogue for primitive mantle-derived, ore-forming magmas to understand the potential for the almost coeval giant gold deposits that display substantial inheritance of mantle volatiles (Mao et al., 2008; Tan et al., 2018).

The < 110 Ma basalts occur at Fuxin (erupted at 100 Ma), Shanwang (18 Ma) and Hebi (4 Ma). Based on their depleted Sr-Nd-Hf isotopes, they are interpreted to be derived from the Mesozoic and Cenozoic convecting asthenospheric mantle (Meng et al., 2015; Zhi et al., 1994; Zhu et al., 2012). The Fuxin basalt is from the northern margin of the eastern NCC and spatially close to the enriched Yixian and Sihetun basalts (Figure 1). The transition from the 130-120 Ma to < 110 Ma basalts in adjacent locations allows comparison of the amount of

253 gold released from the metasomatized SCLM and asthenospheric mantle, respectively. The
254 Shanwang basalts occur near the trans-lithospheric Tanlu fault and the Hebi basalts from the
255 middle part of the NCC where the extent of craton destruction was far less than the eastern
256 NCC. During their eruption, Shanwang and Hebi basalts brought up the mantle xenoliths
257 studied here.

258 The major and trace elements of the basalts from the same locations are generally
259 similar, but the Au and PGEs contents sometimes display a large variation (Figure 2 and
260 DR8). This variation seems not to result from sample heterogeneity as replicate analyses of
261 basalts show consistent values (Figure DR3b). Instead, it reflects the heterogeneous
262 distribution of gold and PGEs in their mantle sources, because Os isotopic compositions of
263 the basalts from the same locations also show a large range (Gao et al., 2008; Huang et al.,
264 2017).

265 Gold contents in the 130-120 Ma and < 110 Ma basalts display positive correlations
266 with PGEs (Figure DR8). Overall, the 130-120 Ma basalts (except those from Fangcheng)
267 show higher Au and PGE contents than the < 110 Ma ones. The low Au contents in the
268 Fangcheng basalts could be attributed to sulfide segregation during magmatic petrogenesis
269 (Sun et al., 2013), but more likely reflect the intrinsic depletion of the mantle source because
270 other chalcophile elements such as Cu and PGEs are also low and Cu/Pd are constant (Figure
271 DR8). The data of Fangcheng basalts thus was excluded to calculate the mean values of 130-
272 120 Ma basalts. The Au/Pd_(N) ratio in the Yixian and Sihetun basalts (erupted at 125 Ma) is
273 slightly higher than that of the adjacent Fuxin basalts (erupted at 100 Ma, Figure DR9), likely
274 suggesting slight enrichment of Au relative to PGEs in the metasomatized SCLM.

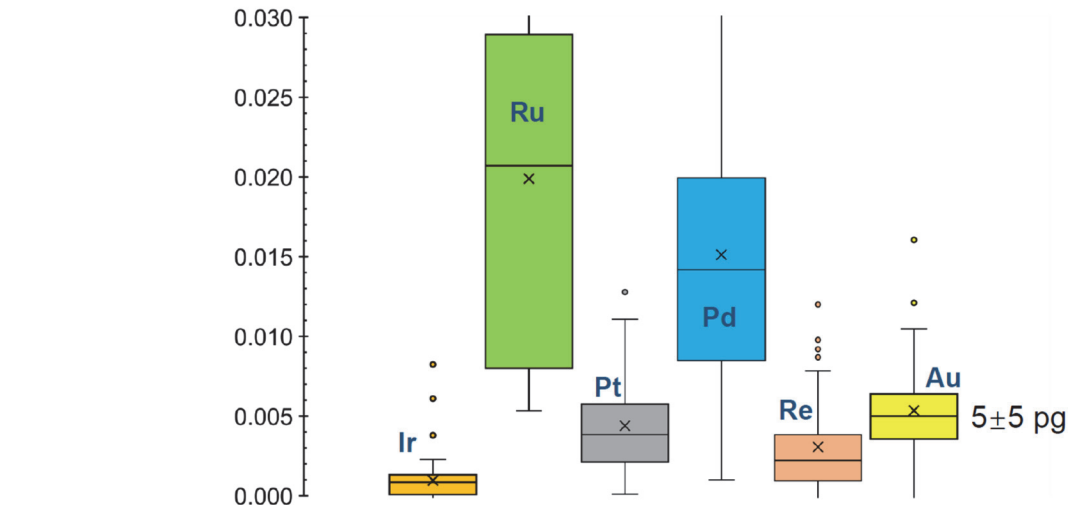
275 The average gold contents from the former are 2.2 ppb, a factor of 3-4 times higher
276 than the 0.7 ppb of the latter, indicating a higher contribution of Au from the metasomatized
277 SCLM, although the metasomatized SCLM was not rich in gold (< 1-2 ppb, Figure 4). The
278 Shanwang basalts located near the trans-lithospheric Tanlu fault contain < 1 ppb Au. The
279 SCLM near Hebi was probably not thinned or thinned to a limited extent (Liu et al., 2011)
280 and the Hebi basalts display similarly low Au contents of < 1 ppb (Figure 2). These results

281 suggest a low Au concentration of the juvenile SCLM or lower extraction efficiency of Au
282 from their mantle source than the metasomatized SCLM.

283 **3.4. High contents of water and volatiles in the 130-120 Ma basalts**

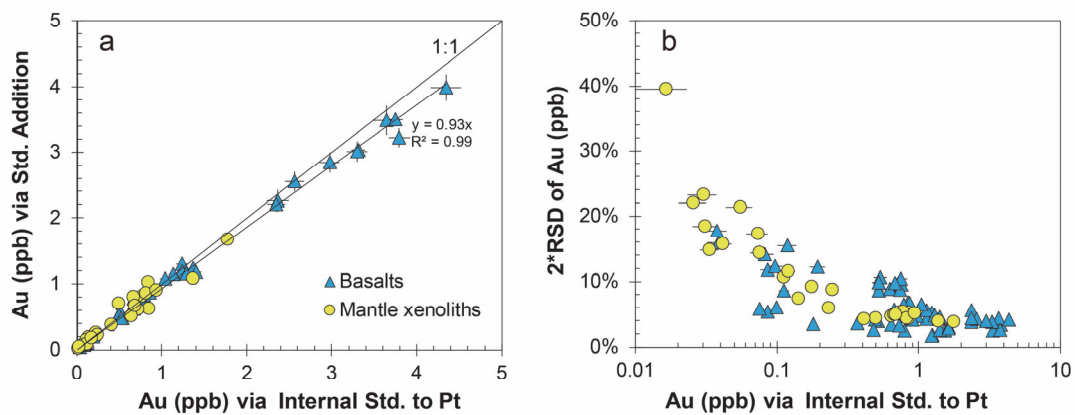
284 The Feixian and Fangcheng basalts are from the southern margin of the eastern NCC,
285 and Yixian and Sihetuan basalts from the northern margin (Figure 1). These 130-120 Ma
286 basalts have been well studied, and were thought to be primitive melts of the metasomatized
287 and hydrated SCLM (Gao et al., 2008; Huang et al., 2017; Liu et al., 2008; Meng et al., 2015;
288 Sun et al., 2013; Xia et al., 2013; Zhang et al., 2002). Previous work has constrained these
289 basalts to be hydrous and volatile-rich (e.g. water, S, C). For example, the Fangcheng basalts
290 show many carbonate and sulfide inclusions and carbon-bearing melt inclusions (Sun et al.,
291 2013). The primitive Feixian basalts contain a few percent water (Xia et al., 2013),
292 suggesting > 1000 ppm water in the metasomatized SCLM source, far higher than the MORB
293 source (50-200 ppm), the Kaapvaal cratonic mantle (120 ppm) (Xia et al., 2013) or the
294 juvenile SCLM of the NCC (Xia et al., 2017). The 130-120 Ma basalts that are from the
295 northern margin of the eastern NCC: the Yixian basalts are also rich in water and volatiles
296 (Geng et al., 2019a; Geng et al., 2019b). Many melt inclusions in olivine phenocrysts display
297 high volatile contents (Figure DR10). Mantle fluids and volatiles promoted gold extraction
298 from mantle during melting and led to elevated gold contents in the hydrous mantle magmas
299 (Botcharnikov et al., 2011; Pokrovski et al., 2013). Given the very high partition coefficients
300 for Au between fluids and hydrous magmas (Pokrovski et al., 2013), fluid exsolution during
301 later magmatic-hydrothermal stage would highly enrich gold in the S, C, Cl and noble gas-
302 bearing fluids. They eventually evolved to auriferous fluids for hydrothermal lode gold
303 deposits. These processes are consistent with the broad similarity in fluid/volatile
304 compositions including C, Cl, and water between hydrous mantle magmas and ore fluids (Qiu
305 et al., 2002; Zhu et al., 2015), and also with the inheritance of a mantle isotopic signature of
306 volatiles and fluids (Mao et al., 2008; Tan et al., 2018).

307

309 **4. Figures DR**

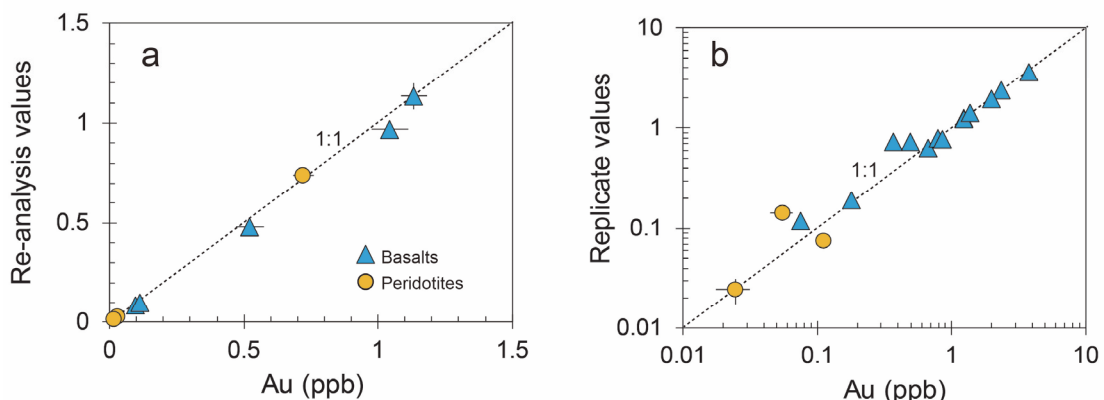
310

311 **Figure DR1.** Total procedural blanks of Au and PGEs in this study (ng), which are negligible
 312 for most samples except samples with low values (e.g., < 0.1 ppb Au). The mean (horizontal
 313 line) and median (cross) values are shown.

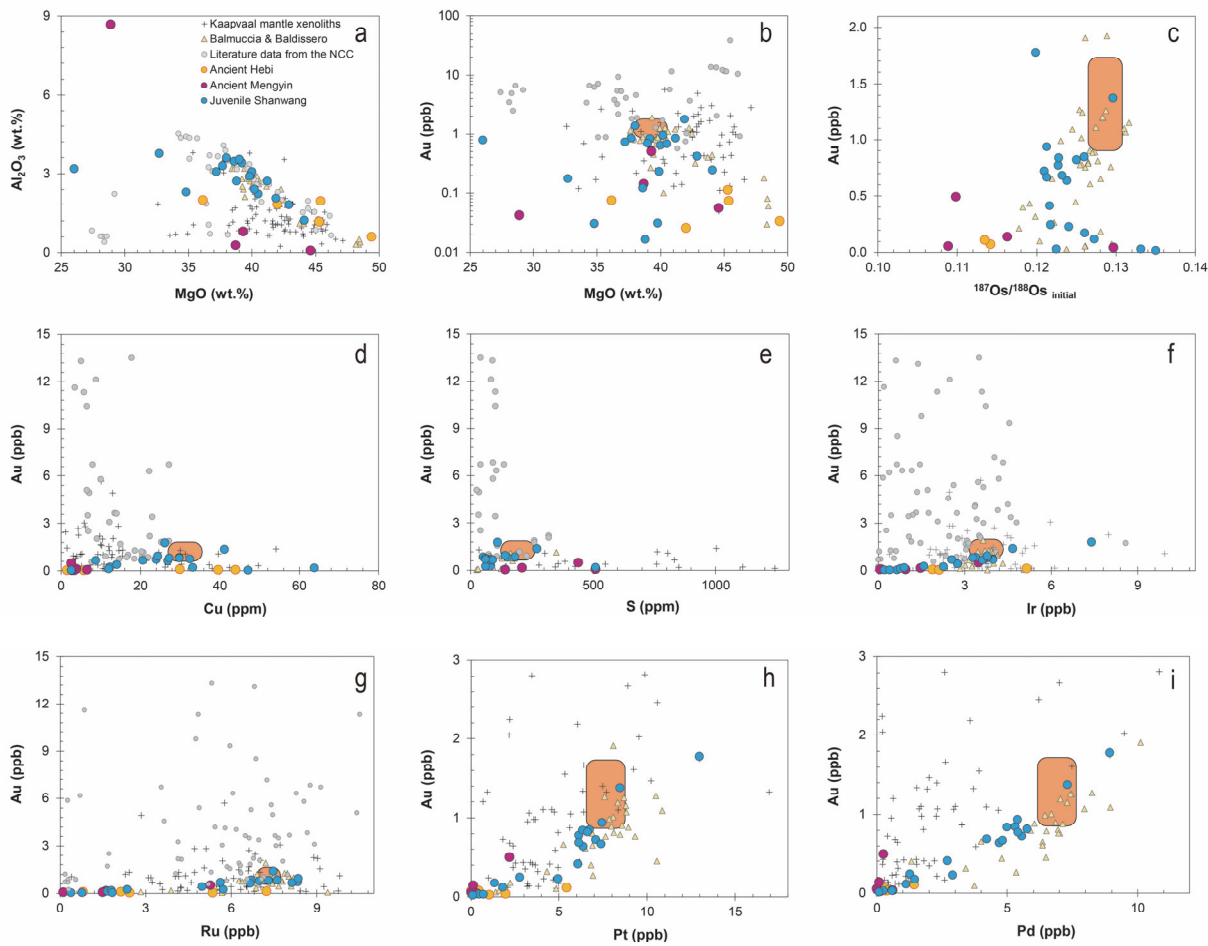


314

315 **Figure DR2.** Comparison of the gold contents obtained by two independent methods: 1)
 316 internal standardization (X axis) and 2) standard addition (Y axis). These two methods
 317 yielded consistent results within a few percent (a). The typical uncertainty is 5-10 % (2sd) for
 318 gold and could be larger for samples with very low contents of < 0.1 ppb (b).



321 **Figure DR3.** Evaluation of data quality of gold contents in this study. a) Re-analyses of
 322 different fractions of aqua regia solution from the same digestion of basalts and peridotites
 323 show reproducible values within analytical uncertainty. b) gold contents of replicates of
 324 eleven basalts and three peridotites which were digested from different fractions of sample
 325 powder, indicating limited effect of sample heterogeneity.



329 **Figure DR4.** Gold and PGE contents in mantle xenoliths from Mengyin, Hebi and Shanwang.

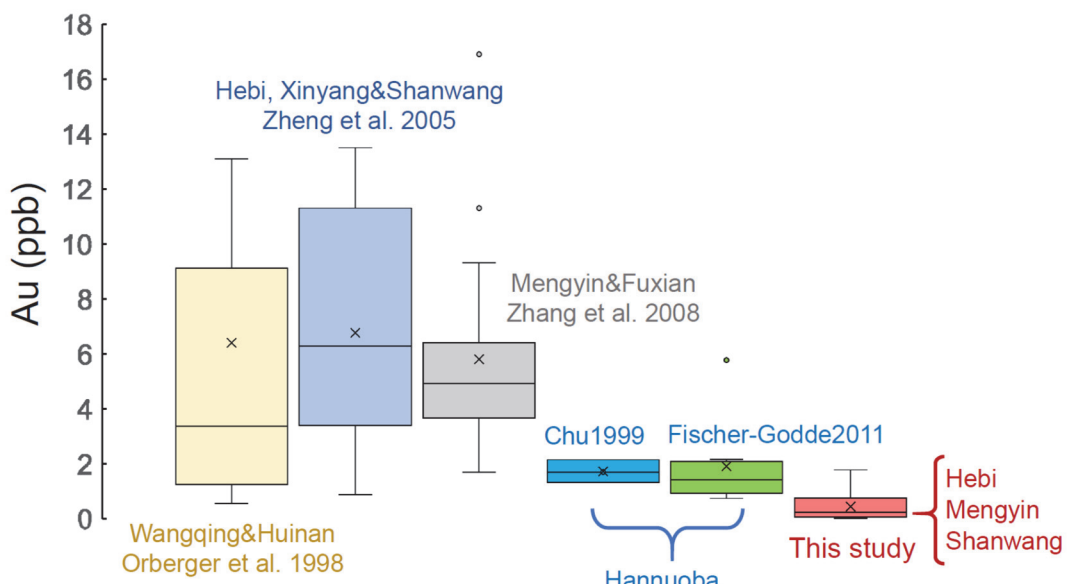
330 Kaapvaal mantle xenoliths (Maier et al., 2012) and massif-type peridotites from Ivrea Zone
 331 (Wang et al., 2013) which were metasomatized or refertilized by sulfide-bearing components,
 332 as well as the estimated range of the primitive mantle ((Becker et al., 2006; Fischer-Gödde et
 333 al., 2011; McDonough and Sun, 1995), orange rectangular) are shown for comparison. The
 334 gold contents, as well as S, Cu, PGEs, of mantle xenoliths from the NCC have reported before
 335 (Chu et al., 1999; Fischer-Gödde et al., 2011; Orberger et al., 1998; Zhang et al., 2008; Zheng
 336 et al., 2005). However, literature gold contents show a large range and overall, noticeably
 337 higher than the new values in this study and those from Kaapvaal, Ivrea Zone and other
 338 locations (Saunders et al., 2018), and do not correlate with S, Cu and PGEs. Note that
 339 Kaapvaal mantle xenoliths show very high S contents but gold contents are near-constant (e).
 340 Literature values from the NCC are not shown in h and i to highlight the similarity in Au and

341 PGE contents between this study and the typical refertilized mantle peridotites. The gold
342 contents in mantle xenoliths of the NCC show good correlations with PGEs.

343

344

Gold contents of this study and previous work



345
346 **Figure DR5.** Comparison of gold contents of this study and previous work on mantle
347 xenoliths from the NCC (Chu et al., 1999; Fischer-Gödde et al., 2011; Orberger et al., 1998;
348 Zhang et al., 2008; Zheng et al., 2005). The literature gold contents show a large range; data
349 from Hannuoba tend to be lower than other locations. The new data on Hebi, Mengyin and
350 Shanwang xenoliths in this study are all lower than older data from the same locations. This
351 study and Fischer-Gödde et al (2011) used the similar analytical methods with low total
352 procedural blanks (a few pg). Note that the values in literature (Orberger et al., 1998; Zhang
353 et al., 2008; Zheng et al., 2005) were obtained by NiS fire assay pre-concentration method.

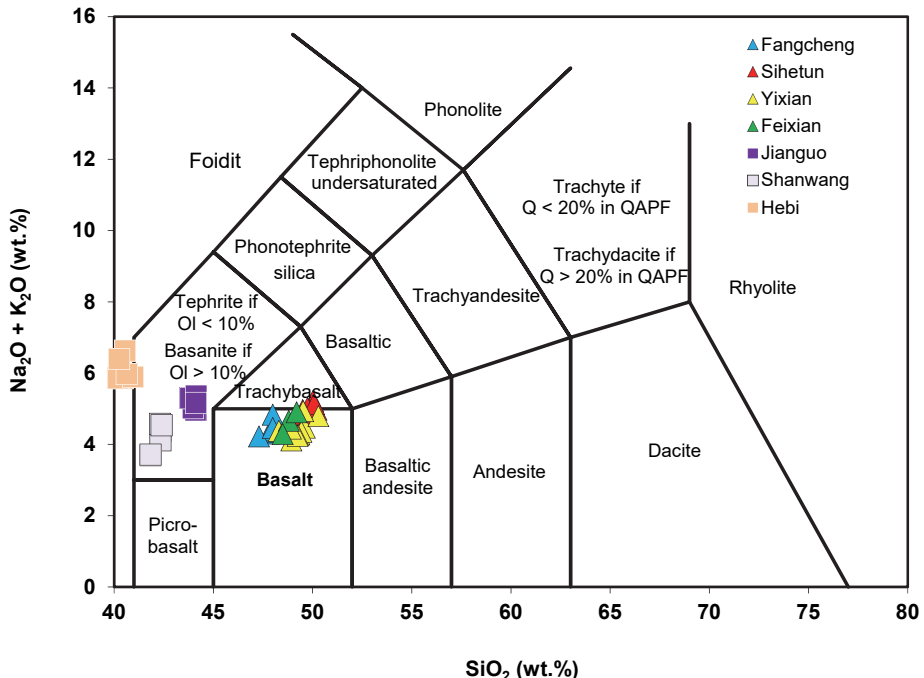
354

355

356

357

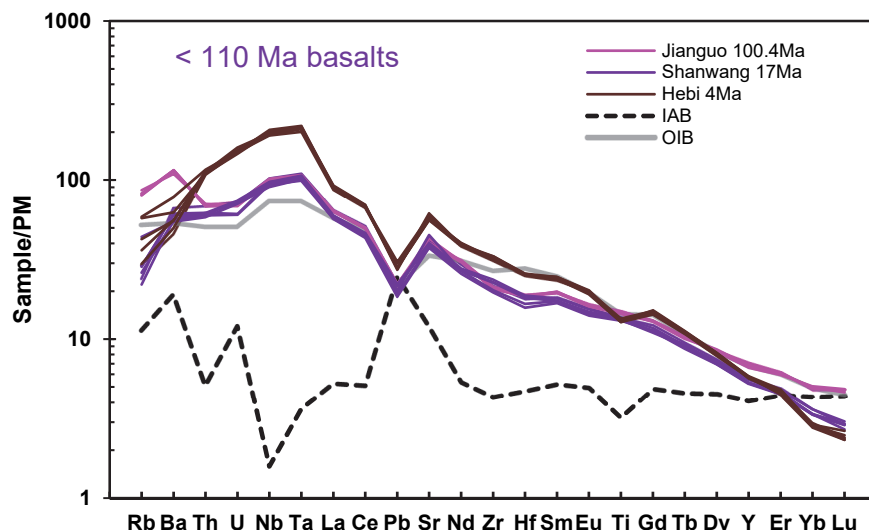
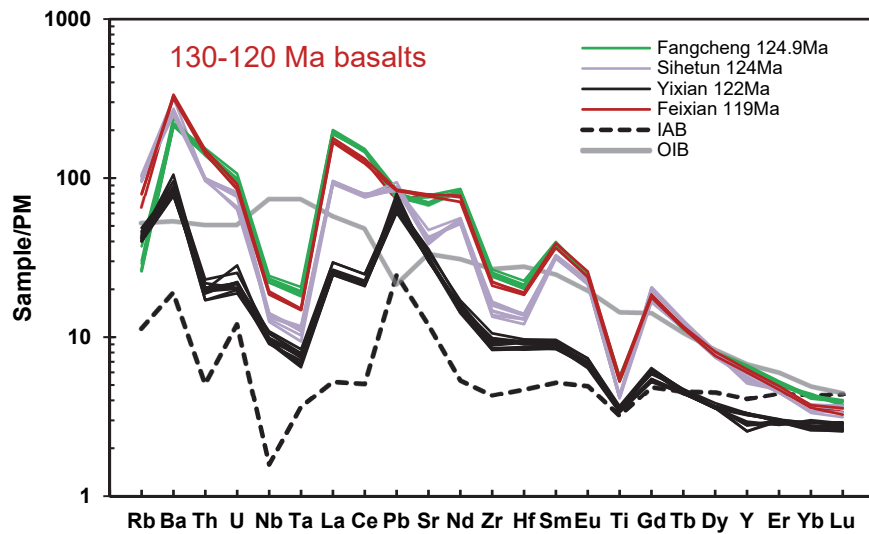
358



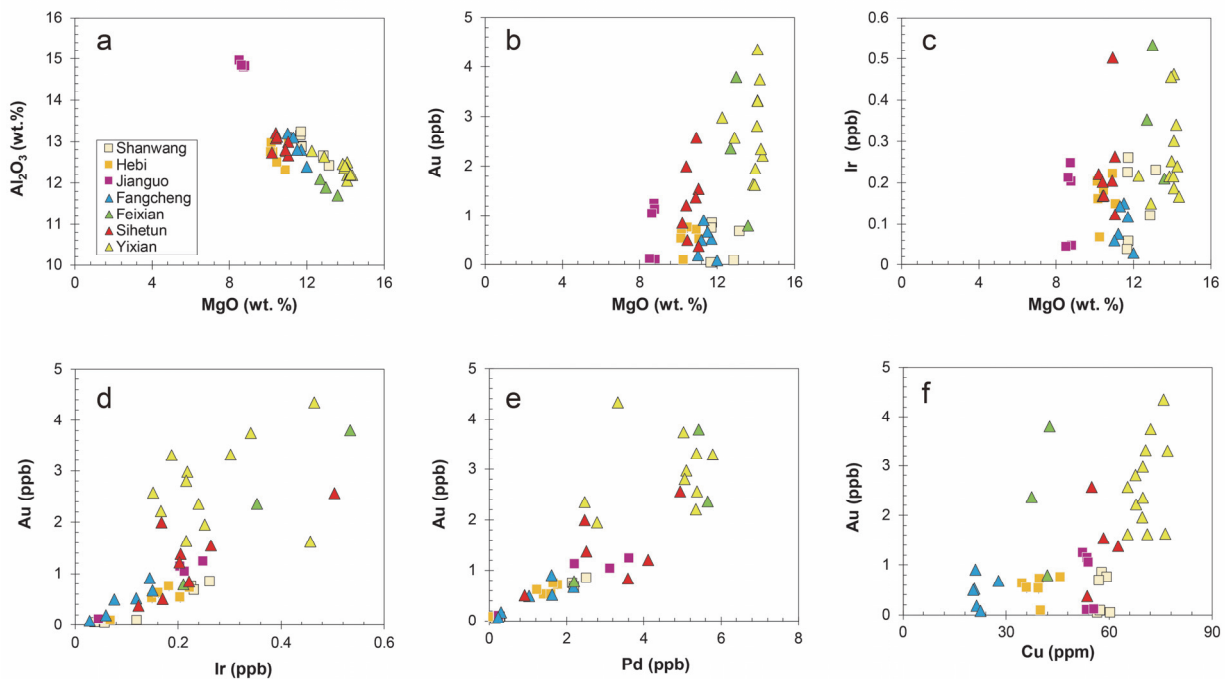
359

360 Figure DR6. Variations in $\text{Na}_2\text{O} + \text{K}_2\text{O}$ vs. SiO_2 (TAS, Le Maitre et al., 1989) for 130-120 Ma
361 and < 110 Ma basaltic samples studied in this study.

362



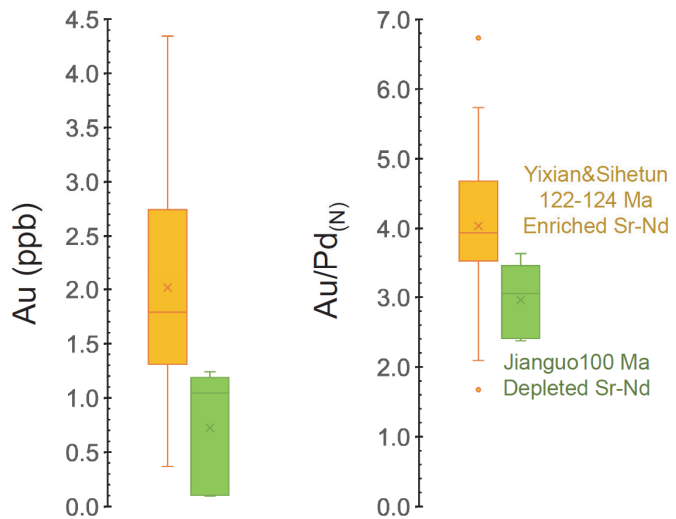
366 **Figure DR7.** Primitive mantle-normalized trace elements patterns of the 130-120 Ma and <
 367 110 Ma basalts. The 130-120 Ma basalts from the metasomatized SCLM show an island arc-
 368 basalt like pattern (depletion of Nb-Ta); whereas the < 110 Ma basalts show an OIB-like
 369 pattern (no depletion of Nb-Ta).



371

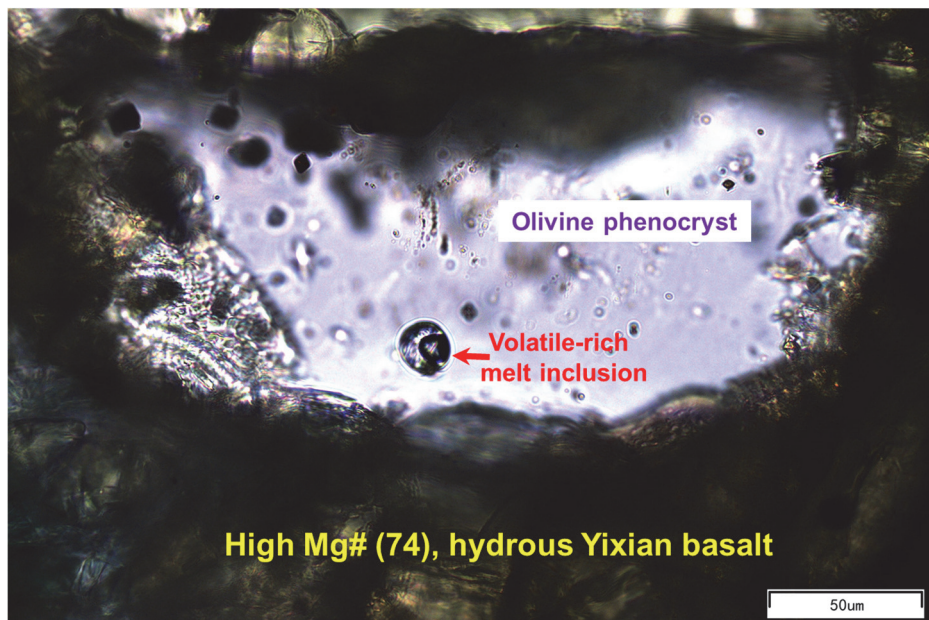
371 **Figure DR8.** Gold and PGE contents of the 130-120 Ma and < 110 Ma basalts. The gold contents show
 372 broadly positive correlations with PGE and Cu contents. Overall, the Au and PGE contents in the 130-
 373 120 Ma basalts from the metasomatized SCLM (triangles) are higher than those of the < 110 Ma
 374 basalts from the juvenile mantle (squares).

375



376

377 **Figure DR9.** Comparison of Au contents and $\text{Au}/\text{Pd}_{(\text{N})}$ in spatially adjacent basalts that
 378 originated from mantle sources with enriched (Yixian and Sihetun) and depleted (Jiangguo) Sr-
 379 Nd isotopes, respectively. The enriched basalts show higher Au contents and $\text{Au}/\text{Pd}_{(\text{N})}$ than
 380 the depleted basalts.



381

382 **Figure DR10:** Volatile-rich, hydrous 130-120 Ma basalts derived from the metasomatized
383 SCLM. Volatile-rich melt inclusions are often present in the early crystallized olivine
384 phenocryst of the primitive, hydrous, isotopically enriched basalts (erupted at 125 Ma). Here
385 shown is the Yixian basalt YX-25 with bulk rock Mg# of 74 and olivine Mg# of 88-91 (Geng
386 et al., 2019a) and bulk rock gold of 3.3 ppb.

387

388 **5. References**

- 389 Barefoot, R. R., and Van Loon, J. C., 1999, Recent advances in the determination of the platinum group
390 elements and gold: *Talanta*, v. 49, no. 1, p. 1-14.
- 391 Becker, H., Horan, M. F., Walker, R. J., Gao, S., Lorand, J.-P., and Rudnick, R. L., 2006, Highly
392 siderophile element composition of the Earth's primitive upper mantle: Constraints from new
393 data on peridotite massifs and xenoliths: *Geochimica et Cosmochimica Acta*, v. 70, no. 17, p.
394 4528-4550.
- 395 Botcharnikov, R. E., Linnen, R. L., Wilke, M., Holtz, F., Jugo, P. J., and Berndt, J., 2011, High gold
396 concentrations in sulphide-bearing magma under oxidizing conditions: *Nature Geoscience*, v.
397 4, no. 2, p. 112-115.
- 398 Brenan, J. M., Bennett, N. R., and Zajacz, Z., 2016, Experimental Results on Fractionation of the
399 Highly Siderophile Elements (HSE) at Variable Pressures and Temperatures during Planetary
400 and Magmatic Differentiation: *Reviews in Mineralogy and Geochemistry*, v. 81, no. 1, p. 1-87.
- 401 Cheng, H., Wang, Z., Chen, K., Zong, K., Zou, Z., He, T., Hu, Z., Fischer-Gödde, M., and Liu, Y.,
402 2019, High-precision Determination of Gold Mass Fractions in Geological Reference
403 Materials by Internal Standardisation: *Geostandards and Geoanalytical Research*, p.
404 <https://doi.org/10.1111/ggr.12284>.
- 405 Chu, X., Li, X., Xu, J., and Liu, J., 1999, Patterns of platinum-group elements in mantle peridotite,
406 granulite xenoliths and basalt in Hannuoba: *Chinese Science Bulletin*, v. 44, no. 18, p. 1676-
407 1681.
- 408 Chu, Z. Y., Wu, F. Y., Walker, R. J., Rudnick, R. L., Pitcher, L., Puchtel, I. S., Yang, Y. H., and Wilde,
409 S. A., 2009, Temporal Evolution of the Lithospheric Mantle beneath the Eastern North China
410 Craton: *Journal of Petrology*, v. 50, no. 10, p. 1857-1898.
- 411 Fischer-Gödde, M., Becker, H., and Wombacher, F., 2011, Rhodium, gold and other highly siderophile
412 elements in orogenic peridotites and peridotite xenoliths: *Chemical Geology*, v. 280, no. 3-4, p.
413 365-383.
- 414 Gao, S., Rudnick, R. L., Carlson, R. W., McDonough, W. F., and Liu, Y. S., 2002, Re-Os evidence for
415 replacement of ancient mantle lithosphere beneath the North China craton: *Earth and
416 Planetary Science Letters*, v. 198, no. 3-4, p. 307-322.
- 417 Gao, S., Rudnick, R. L., Xu, W.-L., Yuan, H.-L., Liu, Y.-S., Walker, R. J., Puchtel, I. S., Liu, X.,
418 Huang, H., Wang, X.-R., and Yang, J., 2008, Recycling deep cratonic lithosphere and
419 generation of intraplate magmatism in the North China Craton: *Earth and Planetary Science
420 Letters*, v. 270, no. 1-2, p. 41-53.
- 421 Geng, X., Foley, S. F., Liu, Y., Wang, Z., Hu, Z., and Zhou, L., 2019a, Thermal-chemical conditions of
422 the North China Mesozoic lithospheric mantle and implication for the lithospheric thinning of
423 cratons: *Earth and Planetary Science Letters*, v. 516, p. 1-11.
- 424 Geng, X., Liu, Y., Wang, X.-C., Hu, Z., Zhou, L., and Gao, S., 2019b, The Role of Earth's Deep
425 Volatile Cycling in the Generation of Intracontinental High-Mg Andesites: Implication for
426 Lithospheric Thinning Beneath the North China Craton: *Journal of Geophysical Research:
427 Solid Earth*, v. 124, no. 124, p. <http://doi:10.1029/2018JB016157>.
- 428 Goldfarb, R. J., and Groves, D. I., 2015, Orogenic gold: Common or evolving fluid and metal sources
429 through time: *Lithos*, v. 233, p. 2-26.
- 430 Griffin, W. L., Begg, G. C., and O'Reilly, S. Y., 2013, Continental-root control on the genesis of
431 magmatic ore deposits: *Nature Geosci*, v. 6, no. 11, p. 905-910.

- 432 Gros, M., Lorand, J.-P., and Luguet, A., 2002, Analysis of platinum group elements and gold in
433 geological materials using NiS fire assay and Te coprecipitation; the NiS dissolution step
434 revisited: *Chemical Geology*, v. 185, no. 3–4, p. 179–190.
- 435 Huang, F., Xu, J.-F., Liu, Y.-S., Li, J., Chen, J.-L., and Li, X.-Y., 2017, Re–Os isotope evidence from
436 Mesozoic and Cenozoic basalts for secular evolution of the mantle beneath the North China
437 Craton: *Contributions to Mineralogy and Petrology*, v. 172, no. 5, p. 28.
- 438 Li, J.-W., Bi, S.-J., Selby, D., Chen, L., Vasconcelos, P., Thiede, D., Zhou, M.-F., Zhao, X.-F., Li, Z.-
439 K., and Qiu, H.-N., 2012, Giant Mesozoic gold provinces related to the destruction of the
440 North China craton: *Earth and Planetary Science Letters*, v. 349–350, p. 26–37.
- 441 Li, Q.-L., Wu, F.-Y., Li, X.-H., Qiu, Z.-L., Liu, Y., Yang, Y.-H., and Tang, G.-Q., 2011, Precisely
442 dating Paleozoic kimberlites in the North China Craton and Hf isotopic constraints on the
443 evolution of the subcontinental lithospheric mantle: *Lithos*, v. 126, no. 1, p. 127–134.
- 444 Liu, J., Rudnick, R. L., Walker, R. J., Gao, S., Wu, F.-y., Piccoli, P. M., Yuan, H., Xu, W.-l., and Xu,
445 Y.-G., 2011, Mapping lithospheric boundaries using Os isotopes of mantle xenoliths: An
446 example from the North China Craton: *Geochimica et Cosmochimica Acta*, v. 75, no. 13, p.
447 3881–3902.
- 448 Liu, Y., Gao, S., Kelemen, P. B., and Xu, W., 2008, Recycled crust controls contrasting source
449 compositions of Mesozoic and Cenozoic basalts in the North China Craton: *Geochimica et
450 Cosmochimica Acta*, v. 72, no. 9, p. 2349–2376.
- 451 Lorand, J. P., Luguet, A., and Alard, O., 2008, Platinum-group elements: A new set of key tracers for
452 the earth's interior: *Elements*, v. 4, no. 4, p. 247–252.
- 453 Lorand, J. P., Luguet, A., and Alard, O., 2013, Platinum-group element systematics and petrogenetic
454 processing of the continental upper mantle: A review: *Lithos*, v. 164–167, no. 0, p. 2–21.
- 455 Luguet, A., Shirey, S. B., Lorand, J. P., Horan, M. F., and Carlson, R. W., 2007, Residual platinum-
456 group minerals from highly depleted harzburgites of the Lherz massif (France) and their role
457 in HSE fractionation of the mantle: *Geochimica et Cosmochimica Acta*, v. 71, no. 12, p. 3082–
458 3097.
- 459 Ma, L., Jiang, S.-Y., Hofmann, A. W., Dai, B.-Z., Hou, M.-L., Zhao, K.-D., Chen, L.-H., Li, J.-W., and
460 Jiang, Y.-H., 2014, Lithospheric and asthenospheric sources of lamprophyres in the Jiaodong
461 Peninsula: A consequence of rapid lithospheric thinning beneath the North China Craton?:
462 *Geochimica et Cosmochimica Acta*, v. 124, p. 250–271.
- 463 Ma, L., Jiang, S.-Y., Hofmann, A. W., Xu, Y.-G., Dai, B.-Z., and Hou, M.-L., 2016, Rapid lithospheric
464 thinning of the North China Craton: New evidence from cretaceous mafic dikes in the
465 Jiaodong Peninsula: *Chemical Geology*, v. 432, p. 1–15.
- 466 Maier, W. D., Peltonen, P., McDonald, I., Barnes, S. J., Barnes, S.-J., Hatton, C., and Viljoen, F., 2012,
467 The concentration of platinum-group elements and gold in southern African and Karelian
468 kimberlite-hosted mantle xenoliths: Implications for the noble metal content of the Earth's
469 mantle: *Chemical Geology*, v. 302, p. 119–135.
- 470 Mao, J., Wang, Y., Li, H., Pirajno, F., Zhang, C., and Wang, R., 2008, The relationship of mantle-
471 derived fluids to gold metallogenesis in the Jiaodong Peninsula: Evidence from D–O–C–S
472 isotope systematics: *Ore Geology Reviews*, v. 33, no. 3–4, p. 361–381.
- 473 McDonough, W. F., and Sun, S. S., 1995, The composition of the Earth: *Chemical Geology*, v. 120, no.
474 3–4, p. 223–253.
- 475 Meng, F., Gao, S., Niu, Y., Liu, Y., and Wang, X., 2015, Mesozoic–Cenozoic mantle evolution beneath
476 the North China Craton: A new perspective from Hf–Nd isotopes of basalts: *Gondwana
477 Research*, v. 27, no. 4, p. 1574–1585.

- 478 Mungall, J. E., and Brenan, J. M., 2014, Partitioning of platinum-group elements and Au between
479 sulfide liquid and basalt and the origins of mantle-crust fractionation of the chalcophile
480 elements: *Geochimica et Cosmochimica Acta*, v. 125, no. 0, p. 265-289.
- 481 Oguri, K., Shimoda, G., and Tatsumi, Y., 1999, Quantitative determination of gold and the platinum-
482 group elements in geological samples using improved NiS fire-assay and tellurium
483 coprecipitation with inductively coupled plasma-mass spectrometry (ICP-MS): *Chemical
484 Geology*, v. 157, no. 3-4, p. 189-197.
- 485 Orberger, B., Xu, Y., and Reeves, S. J., 1998, Platinum group elements in mantle xenoliths from
486 eastern China: *Tectonophysics*, v. 296, no. 1-2, p. 87-101.
- 487 Pitcairn, I. K., Skelton, A. D. L., and Wohlgemuth-Ueberwasser, C. C., 2015, Mobility of gold during
488 metamorphism of the Dalradian in Scotland: *Lithos*, v. 233, p. 69-88.
- 489 Pokrovski, G. S., Borisova, A. Y., and Bychkov, A. Y., 2013, Speciation and Transport of Metals and
490 Metalloids in Geological Vapors: *Reviews in Mineralogy and Geochemistry*, v. 76, no. 1, p.
491 165-218.
- 492 Qiu, Y., Groves, D. I., McNaughton, N. J., Wang, L.-g., and Zhou, T., 2002, Nature, age, and tectonic
493 setting of granitoid-hosted, orogenic gold deposits of the Jiaodong Peninsula, eastern North
494 China craton, China: *Mineralium Deposita*, v. 37, no. 3, p. 283-305.
- 495 Richardson, T., and Burnham, O., 2002, Precious metal analysis at the Geoscience Laboratories: results
496 from the new low-level analytical facility: *Ontario Geol Surv Open File Rep 6100:35*.
- 497 Saunders, E., Pearson, N. J., O'Reilly, S. Y., and Griffin, W. L., 2018, Gold in the mantle: A global
498 assessment of abundance and redistribution processes: *Lithos*, v. 322, p. 376-391.
- 499 Sun, H., Xiao, Y., Gao, Y., Lai, J., Hou, Z., and Wang, Y., 2013, Fluid and melt inclusions in the
500 Mesozoic Fangcheng basalt from North China Craton: implications for magma evolution and
501 fluid/melt-peridotite reaction: *Contributions to Mineralogy and Petrology*, v. 165, no. 5, p.
502 885-901.
- 503 Sun, J., Liu, C.-Z., Wu, F.-Y., Yang, Y.-H., and Chu, Z.-Y., 2012, Metasomatic origin of
504 clinopyroxene in Archean mantle xenoliths from Hebi, North China Craton: Trace-element
505 and Sr-isotope constraints: *Chemical Geology*, v. 328, p. 123-136.
- 506 Tan, J., Wei, J., He, H., Su, F., Li, Y., Fu, L., Zhao, S., Xiao, G., Zhang, F., Xu, J., Liu, Y., Stuart, F.
507 M., and Zhu, R., 2018, Noble gases in pyrites from the Guocheng-Liaoshang gold belt in the
508 Jiaodong province: Evidence for a mantle source of gold: *Chemical Geology*, v. 480, p. 105-
509 115.
- 510 Wan, L., Zeng, Z., Kusky, T., Asimow, P., He, C., Liu, Y., Yang, S., and Xu, S., 2019, Geochemistry
511 of middle-late Mesozoic mafic intrusions in the eastern North China Craton: New insights on
512 lithospheric thinning and decratonization: *Gondwana Research*, v. 73, p. 153-174.
- 513 Wang, Z., and Becker, H., 2015a, Abundances of Ag and Cu in mantle peridotites and the implications
514 for the behavior of chalcophile elements in the mantle: *Geochimica et Cosmochimica Acta*, v.
515 160, no. 0, p. 209-226.
- 516 -, 2015b, Fractionation of highly siderophile and chalcogen elements during magma transport in the
517 mantle: Constraints from pyroxenites of the Balmuccia peridotite massif: *Geochimica et
518 Cosmochimica Acta*, v. 159, no. 0, p. 244-263.
- 519 Wang, Z., Becker, H., and Gawronski, T., 2013, Partial re-equilibration of highly siderophile elements
520 and the chalcogens in the mantle: A case study on the Baldissero and Balmuccia peridotite
521 massifs (Ivrea Zone, Italian Alps): *Geochimica Et Cosmochimica Acta*, v. 108, p. 21-44.
- 522 Wu, F.-Y., Yagn, J.-H., Xu, Y.-g., Wilde, S. A., and Walker, R. J., 2019, Destruction of the North
523 China Craton in the Mesozoic: *Annual Review of Earth and Planetary Sciences*, v. 47, no. 1, p.
524 173-195.

- 525 Xia, Q.-K., Liu, J., Kovács, I., Hao, Y.-T., Li, P., Yang, X.-Z., Chen, H., and Sheng, Y.-M., 2017,
526 Water in the upper mantle and deep crust of eastern China: concentration, distribution and
527 implications: National Science Review, p. nwx016-nwx016.
- 528 Xia, Q.-K., Liu, J., Liu, S.-C., Kovács, I., Feng, M., and Dang, L., 2013, High water content in
529 Mesozoic primitive basalts of the North China Craton and implications on the destruction of
530 cratonic mantle lithosphere: Earth and Planetary Science Letters, v. 361, p. 85-97.
- 531 Xu, Y.-G., Ma, J.-L., Huang, X.-L., Iizuka, Y., Chung, S.-L., Wang, Y.-B., and Wu, X.-Y., 2004, Early
532 Cretaceous gabbroic complex from Yinan, Shandong Province: petrogenesis and mantle
533 domains beneath the North China Craton: International Journal of Earth Sciences, v. 93, no. 6,
534 p. 1025-1041.
- 535 Zhang, H.-F., Goldstein, S. L., Zhou, X.-H., Sun, M., Zheng, J.-P., and Cai, Y., 2008, Evolution of
536 subcontinental lithospheric mantle beneath eastern China: Re-Os isotopic evidence from
537 mantle xenoliths in Paleozoic kimberlites and Mesozoic basalts: Contributions to Mineralogy
538 and Petrology, v. 155, no. 3, p. 271-293.
- 539 Zhang, H.-F., Sun, M., Zhou, X.-H., Fan, W.-M., Zhai, M.-G., and Yin, J.-F., 2002, Mesozoic
540 lithosphere destruction beneath the North China Craton: evidence from major-, trace-element
541 and Sr-Nd-Pb isotope studies of Fangcheng basalts: Contributions to Mineralogy and
542 Petrology, v. 144, no. 2, p. 241-254.
- 543 Zheng, J., Sun, M., Zhou, M.-F., and Robinson, P., 2005, Trace elemental and PGE geochemical
544 constraints of Mesozoic and Cenozoic peridotitic xenoliths on lithospheric evolution of the
545 North China Craton: Geochimica et Cosmochimica Acta, v. 69, no. 13, p. 3401-3418.
- 546 Zheng, J. P., Griffin, W. L., O'Reilly, S. Y., Yu, C. M., Zhang, H. F., Pearson, N., and Zhang, M., 2007,
547 Mechanism and timing of lithospheric modification and replacement beneath the eastern North
548 China Craton: Peridotitic xenoliths from the 100 Ma Fuxin basalts and a regional synthesis:
549 Geochimica et Cosmochimica Acta, v. 71, no. 21, p. 5203-5225.
- 550 Zhi, X., Chen, D., Zhang, Z., and wang, J., 1994, The neodymium and strontium isotopic compositions
551 of Cenozoic alkalic basalts from Penglai and Lingqu, Shandong Province: Geological review,
552 v. 40, no. 6, p. 526-533.
- 553 Zhu, R., Fan, H., Li, J., Meng, Q., Li, S., and Zeng, Q., 2015, Decratonic gold deposits: Science China
554 Earth Sciences, v. 58, no. 9, p. 1523-1537.
- 555 Zhu, Y., Guangshun, H., and Jinhui, Y., 2012, Sources and petrogenesis of the Cenozoic alkali basalts
556 in Hebi,eastern North China Craton:Geochemical and Sr-Nd-Hf isotopic evidence: Acta
557 Petrologica Sinica, v. 28, no. 12, p. 4064-4076.
- 558
- 559
- 560